ELSEVIER

Contents lists available at ScienceDirect

Geochimica et Cosmochimica Acta

journal homepage: www.elsevier.com/locate/gca



A new vanadium species in black shales: Updated burial pathways and implications



Leibo Bian a,b,c, Anthony Chappaz c,*, Niels H. Schovsbo d, Hamed Sanei a,*

- ^a Lithospheric Organic Carbon (LOC) Group, Department of Geoscience, Aarhus University, Aarhus 8000C, Denmark
- ^b State Key Laboratory of Organic Geochemistry, Guangzhou Institute of Geochemistry, Chinese Academy of Sciences, China
- ^c STARLAB, Department of Earth and Atmospheric Sciences, Central Michigan University, Brooks Hall 314, Mount Pleasant, MI 48859, USA
- ^d Department of Reservoir Geology, Geological Survey of Denmark and Greenland, Copenhagen 1316, Denmark

ARTICLE INFO

Article history: Received 18 April 2022 Accepted 26 September 2022 Available online 30 September 2022 Associate editor: Noah J. Planavsky

Keywords: Vanadium Speciation Synchrotron Alum Shale Lower Paleozoic

ABSTRACT

Examining vanadium (V) geochemistry in organic-rich rocks might provide new insights into the redox evolution of paleo ocean and atmosphere through Earth's history. Previous work, mainly based on experiments and thermodynamic predictions, suggested that V is mainly bound to oxygen (O) atoms and/or O-N (nitrogen) groups with oxidation states ranging from +III to +V, when removed from the water column. This conceptual model represented our understanding of the burial processes of V in sedimentary archives, However, until our study, the speciation of V had not been investigated in ancient sediments. For the first time, micro-focused X-ray Absorption Near Edge Structure (μ-XANES) analysis is applied to characterize V speciation in the late Cambrian - Early Ordovician, organic-rich Alum Shale of the Scandinavian region. The result shows the presence of a new V(+IV)-S structure that largely dominates the V speciation (>80%), subordinated by a V(+III)-O structure (<20%) in our samples deposited under euxinic conditions. The $V(+IV)-S/\sum V$ ratio seems to be influenced by the intensity of euxinic conditions. We suggest that the new V(+IV)-S structure may have been formed under strongly sulfidic conditions. Organic matter is most likely to be the dominant host phase for this newly identified species. Additionally, we propose an updated model describing the processes involved during the burial of V under a wide range of redox conditions. This model shows that the V speciation has the potential to provide a more nuanced picture of the redox conditions that prevailed at the time of deposition.

© 2022 Elsevier Ltd. All rights reserved.

1. Introduction

Vanadium (V) systematics (i.e., examining its concentration and isotopic signature) have emerged as promising paleo-redox proxies that could help better refine the reconstruction of Earth's oxygenation and the intensity of paleo anoxic events (Sahoo et al., 2012; Wu et al., 2015, 2019,2020; Nedrich et al., 2018; Moore et al., 2020; Nielsen, 2020; Chételat et al., 2021; Fan et al., 2021; Chen et al., 2022). Naturally occurring V displays several oxidation states within Earth's surface and two isotopes: ⁵¹V (99.76%) and ⁵⁰V (0.24%) (Nielsen et al., 2011; Wu et al., 2015). High V concentrations in sedimentary archives (>500 ppm) seem to be associated with euxinic conditions (Scott et al., 2017; Kunert et al., 2020), whereas low V concentrations suggest oxic conditions (Algeo and Maynard, 2004).

E-mail addresses: anthony.c@cmich.edu (A. Chappaz), Sanei@geo.au.dk (H. Sanei).

Vanadium is a ubiquitous element in the upper crust and the second most abundant transition metal in seawater (Huang et al., 2015; Schlesinger et al., 2017). The mean concentration of V in the continental crust is 97 ppm, and approximately 20×10^9 g V/year can enter biogeochemical cycles (Schlesinger et al., 2017). The sources of V in sedimentary rocks are mainly from the physical and chemical weathering of continental masses (Huang et al., 2015). Other pathways, such as volcanic activity and aeolian process, can release and transport V in the environment but in rather minor amounts, compared to weathering process (Schlesinger et al., 2017). Within modern seawater, the residence time of V is around 91 ka, much longer than ocean water mixing time (1–2 ka; Nielsen, 2020). Therefore, the V systematics has the potential to examine regional and global redox (e.g., Sahoo et al., 2012, 2016; Moore et al., 2020; Fan et al., 2021).

Within natural water, dissolved V species exhibit three oxidation states (+III, +IV, and +V) (Wanty and Goldhaber, 1992; Algeo and Maynard, 2004; Huang et al., 2015). Vanadium (+V) is prevalent in oxygenated water, where the dominant species at neutral

^{*} Corresponding authors.

pH is presented as the quasi-conservative form of vanadate oxyanions, $H^nVO_4^{(n-3)-}$ (n = 0–3). Under acidic and moderately reducing water conditions, V (+IV) ions represent the predominant species, mainly presented as vanadyl cation (VO^{2+}). Vanadium (+IV) can also occur as the VOOH⁺ species with pH ranging from 6 to 7. Under acidic and strongly reducing conditions, V (+III) is thermodynamically stable in the form of V^{3+} , VOH²⁺, and V (OH)⁺₂ species (Wanty and Goldhaber, 1992). Vanadium (+V) can be reduced to V (+IV) by organic acids. However, the reduction of V(+IV and +V) to V(+III) is thought to require the involvement of dissolved sulfides and in most cases is quite slow (Wanty and Goldhaber, 1992).

A widely accepted mechanism for V sequestration in carbonaceous rocks was proposed by Breit and Wanty (1991). Briefly, V (+V) ions, mainly presented as soluble vanadate species, can be reduced into vanadyl ions via organic acids under suboxic-anoxic conditions (but no sulfides). The vanadyl ions can be subsequently associated with organic matter, adsorbed onto Fe/Mn oxyhydroxides, or form insoluble (oxyhydr) oxides. Under euxinic conditions, thermodynamic calculations predict that V(+IV and +V) can be reduced to V(+III) and form insoluble oxides/hydroxides and/or be incorporated into clay minerals such as illite and smectite (Wanty and Goldhaber, 1992; Peacor et al., 2000). The complexation of V to organic compounds and inorganic ligands can inhibit their reduction (Wanty and Goldhaber, 1992; McCann et al., 2013; Huang et al., 2015).

Hitherto, the widely accepted V depositional mechanism in organic-rich rocks has not been tested against the characterization of natural samples. The current depositional mechanism was formulated using thermodynamic calculations based on finite databases, which do not necessarily represent the complexity of natural systems. Until recently, XAFS (X-ray Absorption Fine Structure) analyses had not been applied in characterizing the V speciation in sedimentary records despite their robust capabilities to provide significant insights in terms of redox state, coordination chemistry, and molecular environments (Ardakani et al., 2020; Hlohowskyj et al., 2021). Although previous experimental and modeling studies proposed the reduction of V(+IV and +V) to V (+III) is thermodynamically possible by dissolved sulfides, a recent study suggested this reaction may not be significant under natural conditions (e.g., Kunert et al., 2020). However, two recent studies that used bulk X-ray Absorption Near Edge Structure (XANES) analysis to determine V speciation showed that V is presented as a mixture of V(+III) and V(+IV) oxides under anoxic conditions in modern sediments (Bennett et al., 2018; Nedrich et al., 2018). A weakness present in both studies was the reference materials used to interpret the V XANES spectra collected. The pool of V standards was limited and contained only V oxides with oxidation states ranging from +V to +III. In spite of more than two decades of active research on V geochemistry, we still ignore the processes involved in the burial of V under sulfidic conditions.

The lower Paleozoic Alum Shale, widely distributed in northwestern Europe, shows a distinct variation of V concentrations in different depositional successions (Schovsbo, 2001; Bian et al., 2021). This provides an unprecedented example to elucidate the process of V accumulation in black shales. Herein, we, for the first time, measure V speciation in sedimentary rocks using microfocused XANES analysis. The objectives of this study were (1) to determine V speciation in the late Cambrian – Early Ordovician Alum Shale, (2) to elucidate the mechanisms responsible for formation of the newly observed V structure, and (3) to propose an updated model to explain V sequestration in shales.

2. Geological setting

The Alum Shale Formation was deposited in the western margin of the Baltic continent (Fig. 1A; Nielsen and Schovsbo, 2007). The deposition of this shale straddles the Miaolingian, Furongian, and Early Ordovician (Schovsbo, 2001; Nielsen and Schovsbo, 2015). The present deposition of this shale covers an approximate area of 100,000 km² in northwestern Europe (Fig. 1B; Nielsen and Schovsbo, 2007, 2011). The thickness of this shale changes from 180 m in the Terne-1 well of Denmark (Schovsbo et al., 2014) to < 0.5 m in parts of Estonia and the St. Petersburg area of Russia (Schuth et al., 2019). The lithology in the late Cambrian is relatively homogenous organic-rich shale, intercalated by carbonate concretions, whereas the Lower Ordovician shale is mainly intercalated with mudstone concretions (Nielsen and Schovsbo, 2015; Bian et al., 2021). It is hypothesized that the regional tectonic uplift during the Miaolingian contributed to the formation of a submarine sill that favored the Alum Shale deposition (Nielsen and Schovsbo, 2015). Nevertheless, the water connection between the Baltoscandian Basin and the Iapetus Ocean was persistent during the late Cambrian (Sturesson et al., 2005; Gill et al., 2021). This situation was inherited in the Early Ordovician, supported by the continuous rise of sea level and the deposition of the Alum Shale moving towards the easternmost area in northern Europe (Schuth et al., 2019; Zhao et al., 2022).

The Alum Shale is highly enriched in organic matter (up to 28.0 wt%; Sanei et al., 2014) and redox sensitive metals (Schovsbo, 2001; Kelley et al., 2017; Bian et al., 2021; Schulz et al., 2021). The organic matter in the Alum Shale is composed of marine type-II kerogen (Bharati et al., 1995; Więcław et al.,

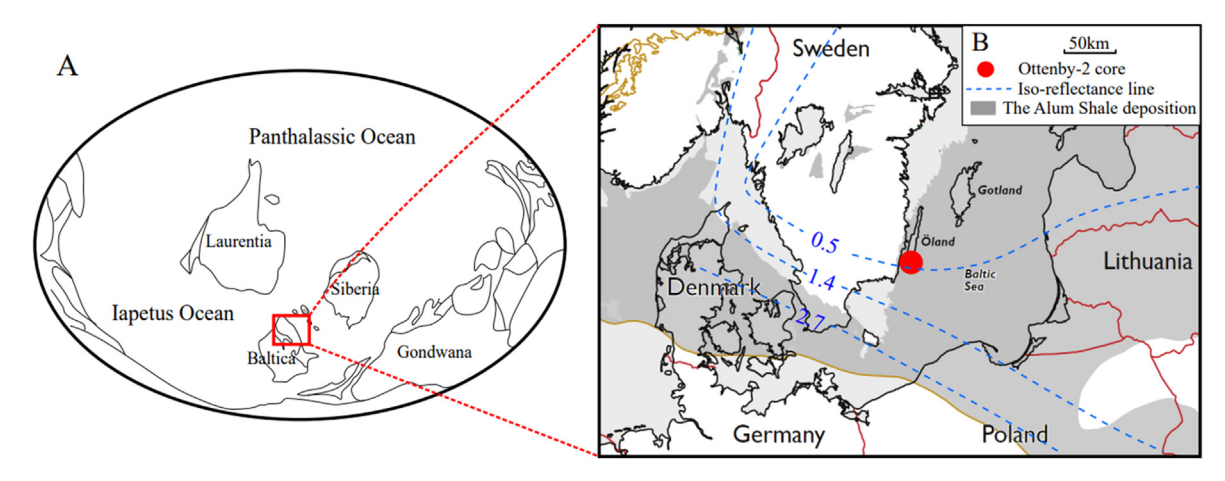


Fig. 1. A: Palaeogeographic reconstruction of the late Cambrian Earth (modified from Scotese, 2001); B: Current distribution of the low Paleozoic Alum Shale and location of the Ottenby-2 core (modified from Nielsen and Schovsbo (2011) and Schovsbo et al. (2014)).

2010; Petersen et al., 2013; Sanei et al., 2014; Zheng et al., 2021). Influenced by multi-stage tectonic activities and magmatic intrusion, the Alum Shale has a wide range of thermal maturity (Fig. 1B; Nielsen and Schovsbo, 2011, 2015). The shale with high thermal maturity is mainly distributed in the eastern part of Norway as well as the southern parts of Denmark and Sweden, whereas the thermal maturity of this shale decreases towards northwestern Europe (Fig. 1; Petersen et al., 2013; Schovsbo et al., 2014).

3. Materials and methods

3.1. Materials

The drilled Ottenby-2 core locates in the southern part of Öland, Sweden (Fig. 1B; GPS Coordinates: 56.14741N, 16.244316E). The lithology of this core is composed of black shale, intercalated with carbonate concretions (Fig. 2). The trilobite biostratigraphy and organic carbon isotopes demonstrate that this core straddles the Miaolingian, Furongian, and Lower Ordovician (Tremadocian) (Bian et al., 2021). The Olenus and Rhabdinopora Superzones are used to mark the tops of the Miaolingian and Furongian, respectively. This core was not influenced by external fluids (Bian et al., 2021) and has a low thermal maturity of organic matter (Fig. 1B; Petersen et al., 2013; Schovsbo et al., 2014).

The Ottenby-2 core was sampled at an interval of approximately 3 samples for each meter. The collected samples were rinsed with distilled water to remove the contamination and then dried at room temperature for 24 h. After that, all samples were pulverized using a corundum mortar and separated into different aliquots for the following experiments.

3.2. Methods

Total organic carbon (TOC), aluminum (Al), molybdenum (Mo), uranium (U), and V contents are compiled from Bian et al. (2021). Sulfur contents and organic carbon isotopes ($\delta^{13}C_{org}$) extend the

late Cambrian dataset of Bian et al. (2022). Total organic carbon contents were measured by the Hawk Pyrolysis (Wildcat Technologies) at Aarhus University. Aluminum (Al), Mo, U, and V contents were measured using the Inductively Coupled Plasmas Mass Spectrometry (ICP-MS) at the ACME Lab. Sulfur contents were measured by the CS230 carbon and sulfur analyzer at Geological Survey of Denmark and Greenland. Organic carbon isotopes were measured by the mass spectrometer (MAT 253 Plus) at Northwest University in China. The analytical procedures and uncertainty of S contents and $\delta^{13} C_{\rm org}$ values can refer to Bian et al. (2022). All data are provided in the supplemental file.

3.2.1. Elemental analysis

Iron (Fe), cadmium (Cd), cobalt (Co), and manganese (Mn) were measured through the ICP-MS at the ACME Lab, Vancouver. About 150 mg samples were digested in a multi-acid combination, including the hydrofluoric (HF), nitric (HNO₃), and perchloric (HClO₄) acids, before evaporated to dryness. After that, the residues were dissolved in the hydrochloric (HCl) acid prior to analysis. The analytical uncertainty was controlled by reference materials (OREAS 45-E), replicates ($\pm 7\%$), and blanks. To calculate enrichment factors of elements, we normalized the concentrations of trace elements to the Post Archean Australia Shale (PAAS) composition (Taylor and McLennan, 1985) by the following formula: $X_{EF} = (X/Al)_{sample}/(X/Al)_{PAAS}$, where X and Al represent concentrations of X and Al in samples and the PAAS.

3.2.2. X-ray Absorption Near Edge Spectroscopy analysis

X-ray Absorption Near Edge Structure (XANES) analysis for determining V speciation was conducted at beamline 13-BM-D at the Advanced Photon Source (APS) of Argonne National Laboratory. Spectra were collected at the V K-edge energy (5,465 eV). At least three spectra per location were collected to improve the signal-to-noise ratio. For each sample, three different locations were selected to account for any heterogeneity. Ultimately, each sample provided nine spectra from 3 distinct locations that were all merged into one. To properly interpret our spectra, five V reference standards, including $V_2(+V)O_5$, $V_2(+IV)O_2$, $V_2(+III)O_3$, $V_3(+IV)O_3$, and $V_3(+III)O_3$, $V_3(+IV)O_3$, and $V_3(+III)O_3$

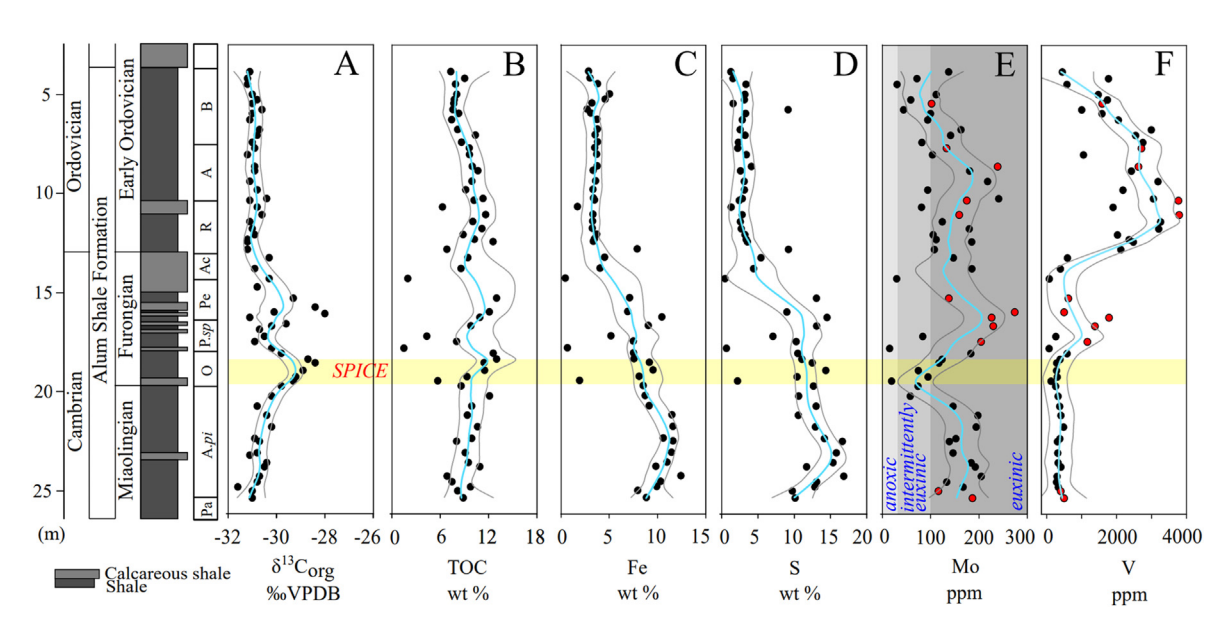


Fig. 2. Profiles of (A) organic carbon isotope ($\delta^{13}C_{org}$), (B) total organic carbon (TOC), (C) Fe, (D) S, (E) Mo, and (F) V concentrations in the Ottenby-2 core with the biostraigraphic profile. The horizontal yellow zone represents the globally recognized Stepoean positive carbon isotope excursion (SPICE) event. In Panel A: Pa: *Paradoxides*; A. pi: *Agnostus pisformis*; O: *Olenus*; P.sp: *Parabolina spinulosa*; Pe; *Petura*; Ac: *Acerocare*; R: *Rhabdinopora* spp. A: *Adelograptus tenellus*; B: *Brygraptus/Kiaerograptus* (Bian et al., 2021). In Panels E and F: Red circles indicate discrete samples for V speciation of X-ray Absorption Fine Structure (XAFS). In Panels A to F: the light blue curve and its 95% confidence level (grey curves) are calculated using a Lowess smoothing (α = 0.15) by the PAST software package. (For interpretation of the references to colour in this figure legend, the reader is referred to the web version of this article.)

were run. The selected samples were marked in Figs. 2 and 4 through red circles. The pre-edge features and the maximum peak (*Em*) obtained from the XANES region were used to determine V oxidation states and coordination chemistry (Tessin et al., 2019). The pre-edge peak is more pronounced for the V=O double bonds but less sensitive to the V=S double bonds and relatively indistinctive for the V=O and V=S single bonds. The *Em* value is correlated positively with V oxidation states and coordination atoms, which was used to calculate the average V oxidation states for each sample. Data processing was conducted by using the Demeter package (Athena). Linear combination fitting (LCF) was applied for the XANES region to determine the predominant V species and their respective amounts. All possible combinations of V standards were tested. For each sample, the combination with the best statistical result was chosen to be representative of the V speciation.

4. Results

4.1. Vanadium concentration and speciation

The bulk concentrations of V display a pronounced increase from 373 ppm (median value) in the Cambrian to 2272 ppm (median value) in the Ordovician (Fig. 2). The pre-edge features and the Em values suggest that the V speciation, for all samples, is quite similar to the VS₂ standard feature with a redox state closer to V (+IV) (Fig. 3). This confirms the first reporting of the occurrence of V(+IV)–S structure in black shales. However, it does not mean that V is presented exactly as VS₂ in our samples, but rather V (+IV) atoms are mostly associated with S atoms in its first shell (Fig. S1). Our LCF results show that, for all samples, two V phases determine the speciation: V(+IV)S₂-like structure and V₂(+III)O₃-like structure, with the V(+IV)–S structure accounting for >80% of V species (Fig. 4D; Table 1). The average oxidation state of V ranges

from 4.00 to 3.82 (Fig. 4B). We can observe that the Cambrian samples have higher ratios of $V(+IV)S_2/\sum V$ (mean = 96%), whereas the ratios are relatively lower in the Ordovician (mean = 84%) (Fig. 4 and Table 1). In addition, Fig. 5 shows that there is a significantly negative correlation between bulk V concentrations and ratios of $V(+IV)S_2/\sum V$ in our samples (R = 0.80, P < 0.05).

4.2. Total iron and sulfur contents

Total iron (Fe) and sulfur (S) contents exhibit similar variations in the profiles (Fig. 2C–D). Iron contents decrease upwards from $\sim\!12.5$ to $\sim\!4.0$ wt% in the Cambrian and remain relatively stable at $\sim\!3.5$ wt% in the Ordovician. Sulfur contents display a significant decrease from $\sim\!16.8$ to $\sim\!5.5$ wt% across the Cambrian and stay $\sim\!3.0$ wt% in the Ordovician. Fig. 6A shows that Fe is significantly correlated to S in the Alum Shale samples (R = 0.96), and Fig. 6B exhibits that there is no relationship between TOC and S.

4.3. Redox condition

Bulk Mo concentrations ([Mo]) are widely used to differentiate redox conditions (Scott and Lyons, 2012). Generally, the following ranges and thresholds, 2 < [Mo] < 25 ppm, 25 < [Mo] < 100 ppm, and [Mo] > 100 ppm, correspond to anoxic conditions, intermittently euxinic conditions, and permanently euxinic conditions, respectively. The samples selected for this study display [Mo] > 100 ppm, suggesting that they were deposited under permanently euxinic conditions (Fig. 2). The enrichment factors of Mo (Mo_{EF}) and U (U_{EF}) can also characterize redox conditions (Taylor and McLennan, 1985; Algeo and Tribovillard, 2009). Fig. 7 displays that both Cambrian and Ordovician samples were deposited under euxinic conditions.

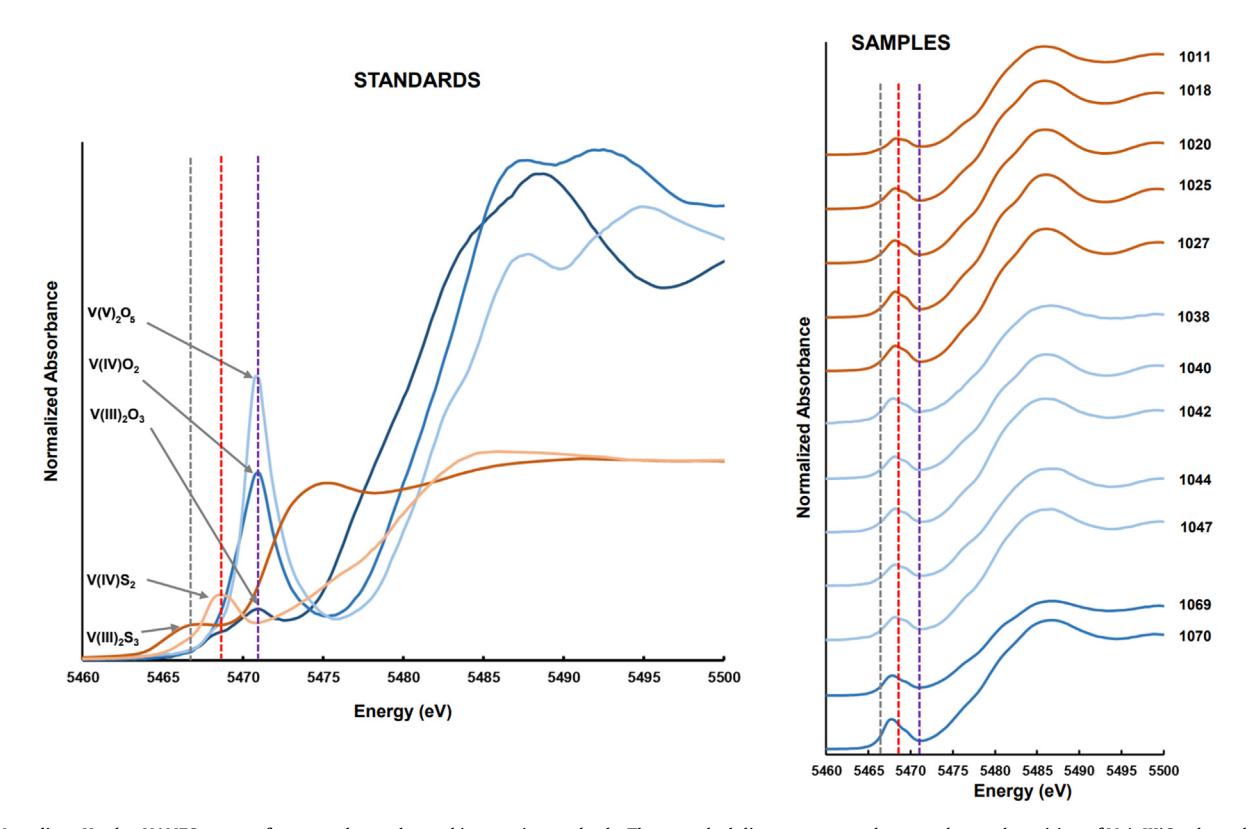


Fig. 3. Vanadium K-edge XANES spectra for natural samples and inorganic standards. The grey dash lines represent the pre-edge peak position of $V_2(+III)S_3$, the red dash line indicates the pre-edge peak position of $V(+IV)S_2$, and the purple dash line means the V-O bond. (For interpretation of the references to colour in this figure legend, the reader is referred to the web version of this article.)

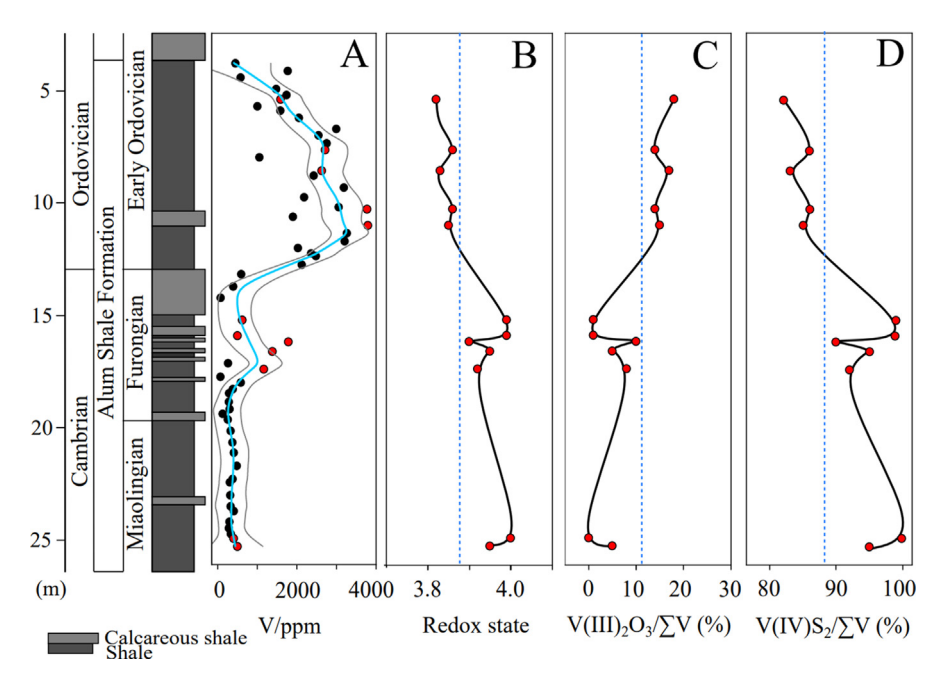


Fig. 4. Profiles of (A) V concentrations, (B) average oxidation state, (C) ratios of $V_2(+III)O_3/\sum V$, and (D) ratios of $V_2(+IV)S_2/\sum V$ in the Ottenby-2 core.

Table 1Analytical results of bulk V concentrations and X-ray Absorption Near Edge Structure (XANES).

Sample	Stage	Depth(m)	V (ppm)	$V_2(+IV)S/\sum V$	$V_2(+III)O_3/\sum V$	Average redox state
1011	Early Ordovician	5.44	1592	0.82	0.18	3.82
1018	Early Ordovician	7.69	2713	0.86	0.14	3.86
1020	Early Ordovician	8.62	2629	0.83	0.17	3.83
1025	Early Ordovician	10.33	3773	0.86	0.14	3.86
1027	Early Ordovician	11.05	3793	0.85	0.15	3.85
1038	Late Cambrian	15.27	621	0.99	0.01	3.99
1040	Late Cambrian	15.96	503	0.99	0.01	3.99
1042	Late Cambrian	16.24	1788	0.90	0.10	3.90
1044	Late Cambrian	16.67	1383	0.95	0.05	3.95
1047	Late Cambrian	17.45	1164	0.92	0.08	3.92
1069	Late Cambrian	24.99	403	1.00	0.00	4.00
1070	Late Cambrian	25.35	499	0.95	0.05	3.95

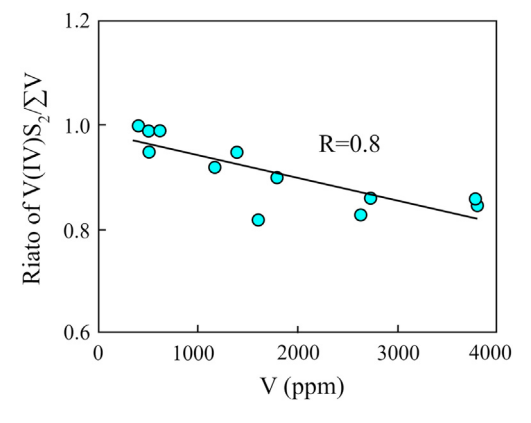


Fig. 5. Ratios of $V(+IV)S_2/\sum V$ versus bulk vanadium concentrations. The significance level is >95%.

4.4. Water circulation and organic matter preservation

The Co \times Mn values and Cd/Mo ratios can be used to distinguish the depositional environment (Sweere et al., 2016). Fig. 8 shows that the Co \times Mn values in the late Cambrian are above

0.4 ppm \times %, whereas the Co \times Mn values are mainly below 0.4 pp m \times % for the Early Ordovician samples. In addition, the Cd/Mo ratios are below 0.03 for the Cambrian samples, while they range mainly between 0.03 and 0.2 in the Ordovician (Fig. 8).

5. Discussion

5.1. The formation of the V(+IV)–S structure

The XANES and LCF results demonstrate that V(+IV)–S structure (>80%) dominates the species of V, followed by V(+III)–O structure (<20%) in our samples (Fig. 4). We consider three mechanisms to explain this observation: (1) the quick transport and deposition of terrigenous clastic inputs (i.e., patronite) that would offer a limited time for the decomposition of those particles within the water column; (2) the natural vulcanization process of organic matter during the diagenetic process (Tegelaar et al. 1989; Wakeham, 1995; Kok et al., 2000; Aycard et al., 2003); and (3) a previously unrecognized dominant structure in black shales, based on the widely accepted V depositional mechanism (Wanty and Goldhaber, 1992).

The quick terrestrial erosion and deposition within a limited time can be excluded (mechanism 1), because previous studies

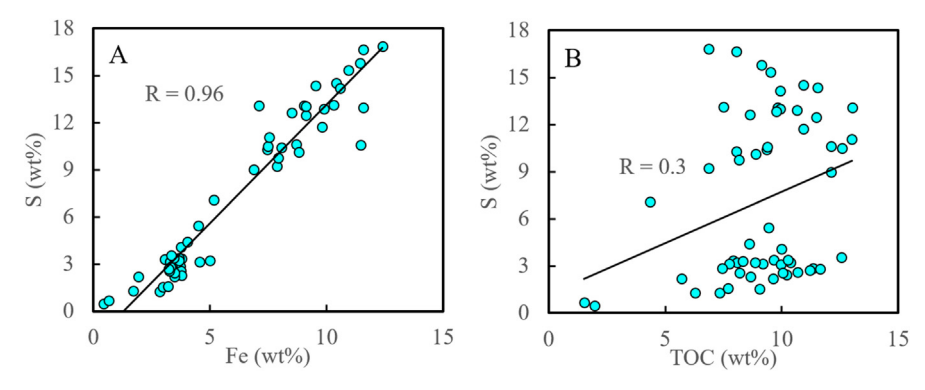


Fig. 6. Crossplots of (A) Fe versus S and (B) TOC versus S.

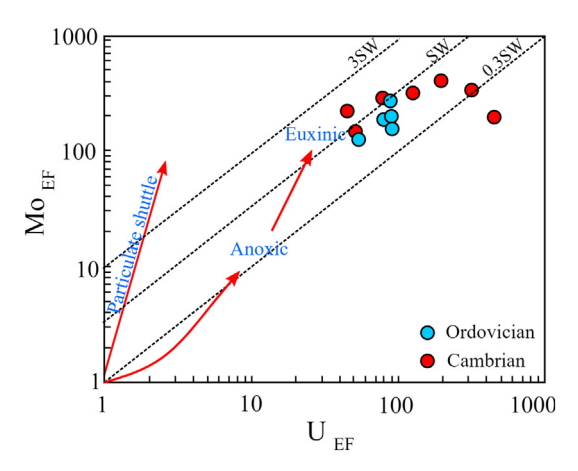


Fig. 7. Enrichment factors of molybdenum (Mo_{EF}) versus uranium (U_{EF}) (Algeo and Maynard, 2004).

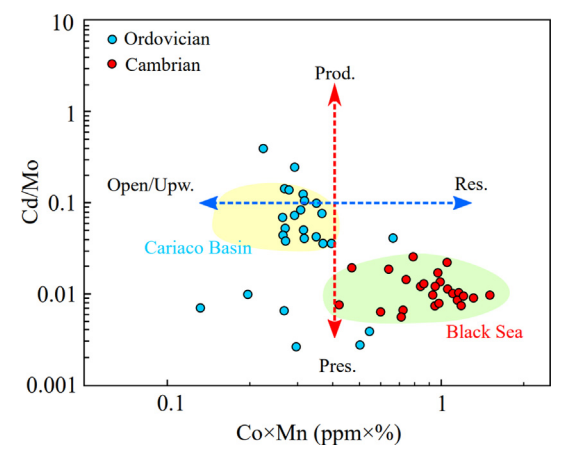


Fig. 8. Crossplot of Cd/Mo ratio versus Co \times Mn value in the Alum Shale. Only samples with Mo exceeding 25 ppm are used (Sweere et al, 2016). Open/Upw.: Open/Upwelling water conditions; Res.: Restricted water conditions; Prod.: Productivity of organic matter; Pres.: Perseveration of organic matter. The red dash line represents the Co \times Mn value is 0.4 ppm \times %, and the blue dash line means the Cd/Mo ratio is 0.1. These two values are suggested in Sweere et al. (2016). (For interpretation of the references to colour in this figure legend, the reader is referred to the web version of this article.)

suggested an extremely low sedimentation rate in the Alum Shale (<10 mm/ka; Sørensen et al., 2020; Zhao et al., 2022) and vanadium sulfides were not identified in the Alum Shale (Loog and Petersell, 1995; Loog et al., 2001).

During the diagenetic process, V is generally considered to be contained in porphyrins and chelated with O/N atoms in organic matter (Breit and Wanty, 1991). Therefore, the V-S species might be formed by replacing O/N atoms in organic compounds. However, it is difficult to conclude the V(+IV)-S structures can account for around 100% V species in the immature/low mature samples (Table 1), given that macro-organic molecular (e.g., porphyrins) are generally preserved during the diagenetic process (e.g., Sanei, 2020) and it is an unrealistic assumption to consider that all the O/N atoms bound to V atoms were replaced. Another potential mechanism could be the formation of sulfur-rich type-II kerogen. This kind of high-molecular-weight, sulfurized organic matter can be formed by the intermolecular incorporation of inorganic S into small organic compounds during the early stage of sedimentary diagenesis (Machel, 2001; Waples, 2013). Such highly sulfurized organic matter is expected to be found in carbonaceous marine sediments with low contents of reactive irons and high abundance of dissolved sulfides (Breit and Wanty, 1991). This natural vulcanization process may be a potential mechanism for forming V(+IV)-S structure through the incorporation of V into sulfurized organic matter. Wiecław et al. (2010) measured organic S/(S + C) ratios in three Alum Shale samples located in southern Öland. Their results showed that organic S/(S + C) ratios are 0.021 and 0.025 in the late Cambrian samples, and it is 0.007 in the Lower Ordovician sample, which indicates that organic matter is not composed of sulfur-rich type-II kerogen. Furthermore, Fig. 6 shows that S is significantly correlated to Fe and not correlated to TOC, suggesting that iron sulfides are dominant host phases for S and that organic matter is not highly sulfurized in the Alum Shale. In addition, Fig. S2 shows that there is no significant relationship between the ratio of $V(+IV)S_2/\sum V$ and free hydrocarbon. This indicates that the formation of V(+IV)-S species was not associated with the thermal evolution of organic matter during the diagenetic process. Therefore, we can reasonably exclude the second mechanism.

In order to examine the third mechanism, the redox conditions were determined using bulk Mo concentrations and enrichment factors of U and Mo (Algeo and Tribovillard, 2009; Scott and Lyons, 2012). Figs. 2 and 5 show that the samples were deposited under euxinic conditions. Given that previous studies characterized the V speciation in modern anoxic settings (i.e., no or low dissolved sulfides) and found that V is mostly presented as the V(III)–O species under anoxic conditions instead of euxinic conditions (Fig. 8; e.g., Bennett et al., 2018), we consider that the formation of V(+IV)–S species in our samples can be attributed to the occurrence of strongly sulfidic conditions.

Fig. 4 shows that the late Cambrian samples have higher V(+IV) $S_2/\sum V$ ratios, ranging between 90% and 100%, while the V(+IV) $S_2/\sum V$ ratios in the Early Ordovician are lower (80–90%). For inter-

preting the changes in $V(+IV)S_2/\sum V$ ratios, we use a cross plot of Co × Mn value and Cd/Mo ratio to make an analogy with modern depositional environments (Sweere et al., 2016). Fig. 8 shows that the late Cambrian samples were deposited into a highly restricted basin with high organic matter preservation, corresponding to the depositional environment of the modern Black Sea, while the Early Ordovician samples were deposited into a moderately restricted basin, corresponding to the depositional environment of the modern Cariaco Basin. Because the contents of dissolved sulfides in the Black Sea and Cariaco Basin can reach 400 µM and 40 µM, respectively (Algeo and Lyons, 2006), we hypothesize that the variations in the relative ratio of V(+IV)-S and V(+III)-O structures may provide a more nuanced approach to improve the characterization of sulfidic conditions (i.e., high vs low level of dissolved sulfides within the water column). Our interpretation of V speciation results for the Early Ordovician samples is in agreement with Kunert et al. (2020) that stated that samples with hyperenrichment of V (>500 ppm) can be deposited under weakly euxinic conditions.

In addition, a significantly negative correlation between bulk V concentrations and $V(+IV)S_2/\sum V$ ratios can be observed in the Alum Shale (Fig. 5). Given that redox metals in metalliferous shales were mainly derived from seawater (Lehmann et al., 2007; Gill et al., 2011) and the low sedimentation rate in the Alum Shale (Sørensen et al., 2020; Zhao et al., 2022), we hypothesize that V in the Alum Shale was mostly supplied by an increased flux of seawater. Vanadium, originally contained in seawater, mainly went through reducing conditions within the water column and was quickly reduced and preserved in sediments. This process could have been responsible for elevated bulk V concentrations in the Alum Shale. Compared to the late Cambrian, the important flux of seawater in the Early Ordovician may have led to significantly increased V concentrations in the Alum Shale but simultaneously weakened the late Cambrian extremely sulfidic conditions (buffer effect).

5.2. The potential host phases of the V(+IV)-S structure

For organic-rich shales with low thermal maturity, V is generally hosted by organic fractions through forming organometallic ligands and/or adsorbing onto organic matter (Emerson and Huested, 1991; Morford and Emerson, 1999; Algeo and Maynard, 2004). In addition, two recent studies showed that V(+V) ions could be reduced by Fe(+II)-minerals such as mackinawite and magnetite (Vessey and Lindsay, 2020; O'Loughlin et al., 2021). Because V(+IV) ions can be incorporated into Fe(+II) minerals by forming bidentate corner-sharing V(+IV)–S structures (Vessey and Lindsay, 2020), the reduction of V by Fe (+II) minerals (i.e., mackinawite) is a potential mechanism for V sequestration. In this study, we specifically focus on exploring the roles of organic matter and Fe(+II) minerals for hosting the V(+IV)–S structure.

Under sulfidic conditions, iron sulfides typically start to form metastable phases, i.e., mackinawite, and later recrystallize to pyrite during the diagenetic and catagenetic processes (Machel, 2001; Rickard and Luther, 2007). The extensive presence of framboidal pyrite has been well documented in the Alum Shale, supporting the quantitative recrystallization of iron monosulfides to pyrite (Petersen et al., 2013; Sanei et al., 2014; Schulz et al., 2021; Zheng et al., 2021). Because pyrite has a negligible effect on fixing V due to their incompatible structures (Wanty and Goldhaber, 1992; Algeo and Maynard, 2004), we suggest that limited amounts of V are hosted by iron sulfides in the Alum Shale. This conclusion is also supported by Fig. 9A–B, which shows that V and S are not correlated in the Cambrian and Ordovician samples.

Fig. 9C–D show that V and TOC are significantly correlated, suggesting that organic matter is mainly responsible for fixation of V.

Given that (1) the direct reduction of V(+V) to V(+IV) by organic acids mainly forms the V(+IV)-O structure, and (2) the natural vulcanization of organic matter during the diagenetic process is not responsible for the formation of the V(+IV)-S structure observed in the Alum Shale, we suggest different levels of sulfide present in the water column influenced the V speciation recorded in the Alum Shale.

5.3. New model for vanadium burial in organic-rich rocks

The current model describing the burial pathways of V indicates the soluble V(+V) ions are being reduced to V(+IV) ions by organic acids and then mainly scavenged by organic matter (Wilson and Weber, 1979; Breit and Wanty, 1991; Algeo and Maynard, 2004). The V(+IV and +V) ions can be reduced to V(+III) ions by dissolved sulfides and then fixed by clay minerals and/or geoprophyrins (Wanty and Goldhaber, 1992; Algeo and Maynard, 2004; Bennett et al., 2018; Nedrich et al., 2018). Recent studies demonstrated the importance of Fe(+II) minerals to sequester V (Vessey and Lindsay, 2020). In this study, we propose a new model (Fig. 10 and Table 2) by combining recent findings with our results:

Under oxygenated settings, V occurs as V(+V)–O species that can precipitate through the adsorption to Fe/Mn oxyhydroxides (Hobson et al., 2018; Gustafsson, 2019; Vessey et al., 2020).

Under nitrogenous and manganous conditions, V(+V) can be reduced to V(+IV) by organic acids such as citric and oxalate acids (Wagner et al., 2017). Vanadium occurs as V(+IV)–O species that are mainly associated with organic matter (e.g., Tribovillard et al., 2006).

In presence of a large amount of dissolved Fe(+II) ions within the water column (ferruginous conditions), Fe (+II) minerals like siderite or magnetite ions would act as reducing agents for V(+V) ions (Vessey and Lindsay, 2020). The newly formed V(+IV) could be either associated with organic matter phases or incorporated into the structure of Fe(+II) minerals (Algeo and Maynard, 2004; Huang et al., 2015; Vessey and Lindsay, 2020).

Under stronger reducing conditions than ferruginous conditions but weaker than euxinia, V(+V) could be reduced by Fe(+II)-sulfur minerals (i.e., mackinawite). As the redox condition becomes more reducing (weak euxinia), V(+IV) species would react with the low concentration of sulfides available and form V(+III)–O species and elemental sulfur as products. Shortly after, V(+III) could be rapidly reacted with V(+V) and form V(+IV) species until all the V(+V) is consumed (Yang and Gould, 2003). We suggest that V species are mainly presented as V(+IV)–O and V(+III)–O structures under anoxic conditions. The major host phase of V (+IV) species is organic matter, whereas the V(+III) would be either incorporated into clay minerals by replacing Al³⁺ ions, associated with organic matter, or form V oxyhydroxides (Algeo and Maynard, 2004; Huang et al., 2015; Vessey and Lindsay, 2020).

In presence of high level of dissolved sulfides (euxinic conditions), the V(+IV)–S structure would form. Unlike the mechanism described above for anoxic conditions, we propose that V(+V) would be directly reduced by sulfide to form the V(+IV)–S structure that would be subsequently associated with the preserved organic matter. Our speciation results identify the V(+IV)–S structure as the main V species that would form under strongly sulfidic conditions, while the V(+III)–O structure (that represents at the most 20% of the V speciation) would begin to form under weakly euxinic conditions.

5.4. Implications for utilizing V as paleo-redox proxies

A new V(+IV)-S species is identified in the organic-rich Alum Shale deposited under euxinic conditions. Characterizing the V speciation can provide a more nuanced picture of the redox condi-

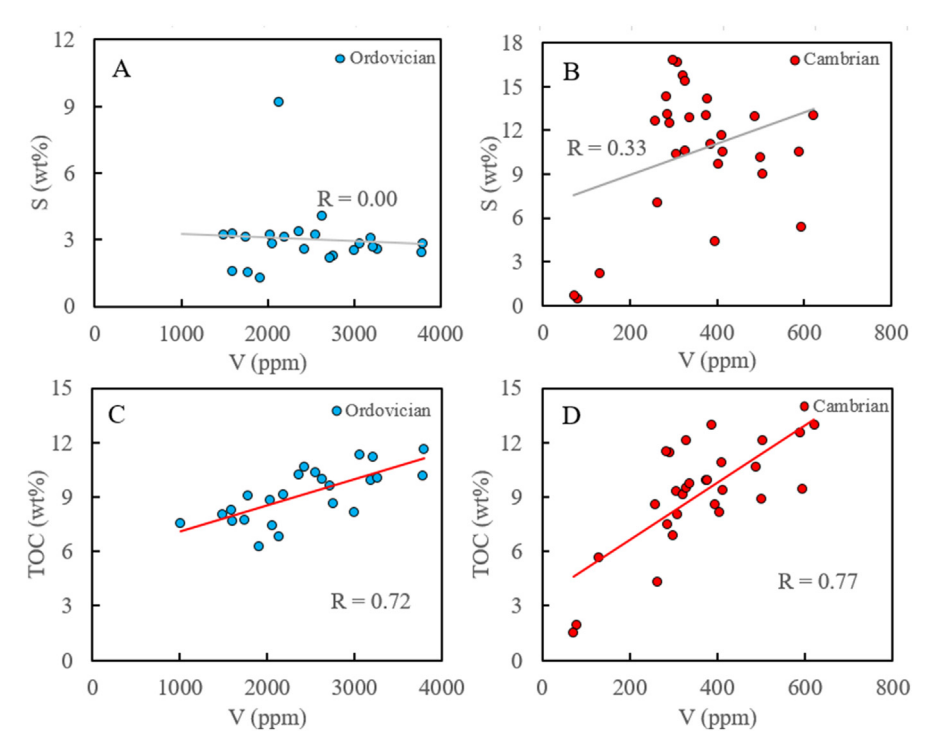


Fig. 9. Crossplots of (A) V versus Fe in the Ordovician samples, (B) V versus Fe in the Cambrian samples, (C) V versus Fe in the Ordovician samples, and (D) V versus Fe in the Cambrian samples.

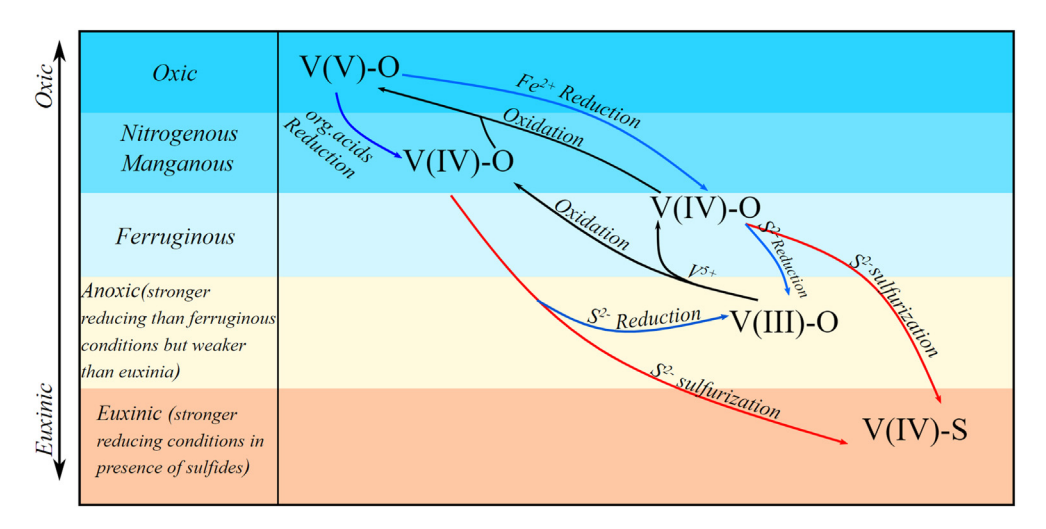


Fig. 10. Summary for V burial pathways in carbonaceous rocks. The V burial mechanism is built based on this study and previous studies (Wanty and Goldhaber, 1992; Yang and Gould, 2003; Nedrich et al., 2018; Vessey and Lindsay, 2020).

 Table 2

 Proposed mechanisms for the formation of various vanadium structures under different depositional environments. DOM: dissolved organic matter; POM: particulate organic matter.

	Organic matter	S(-II)	Dissolved /solid Fe(II)	Redox condition	Reductive pathway
V(+V)-O	Unreactive DOM	No	No	Oxic	No
V(+IV)-O	DOM	No	No	Nitrogenous/Mangenous	Organic acids
V(+IV)-O	DOM	No	Yes	Ferruginous	Organic acids; Fe(II)
V(+III)-O	DOM; Unreactive POM	Limited	Yes	Stronger reducing than ferruginous and weaker than euxinia	Organic acids; Fe(II); S(-II)
V(+IV)-S	POM	Yes	No dissolved Fe(II)	Stronger reducing conditions in presence of sulfides	Organic acids; Fe(II); S(-II)

tions prevailing at the time of deposition, specifically allowing to differentiate between weak and strong euxinia. Although these first results are encouraging, the complexity of the V burial processes in organic-rich shales – influenced by the content and ther-

mal maturity of organic matter, redox conditions, concentrations of sulfate and iron ions, and microbiological activities (aerobic vs anaerobic) – calls for additional studies. However, the potential of the V speciation as a paleo-redox proxy is very promising

because it exhibits several oxidation states and different bonding structures that could provide more subtility in our efforts to capture past redox conditions.

6. Conclusions

We propose a new model to explain the mechanisms involved during V burial in organic-rich rocks deposited under various redox conditions. In this study, we use X-ray Absorption Near Edge Structure to determine V speciation in the organic-rich Cambrian-Ordovician Alum Shale. Our results show the occurrence of a new V(+IV)-S structure in the Alum Shale. The V(+IV)-S structure is the dominant V species ranging from 80% to 100%, whereas the ratio of V(+III)-O structure accounts for <20%. We consider that the formation of V(+IV)-S structure is likely attributed to the presence of strongly sulfidic conditions and that the relative ratio of V $(+IV)-S/\sum V$ may be influenced by the level of sulfide available in the water column. We identify organic matter as the main host phase of V. We infer that, under strongly sulfidic conditions, sulfides could have reduced V(+V) to V(+IV) bound to S atoms. Subsequently, this new V(+IV)-S structure would be incorporated into organic matter. Further work is required to confirm/object to our assumption. Characterizing V speciation in sedimentary records has the potential to introduce more nuance into the identification of past redox conditions.

Data availability

Data will be made available on request.

Declaration of Competing Interest

The authors declare that they have no known competing financial interests or personal relationships that could have appeared to influence the work reported in this paper.

Acknowledgements

All authors thank help from Dr. Carsten Guvard of GEUS for technical assistance. Great gratitude goes to the financial supports from GeoCenter Denmark Project 2017-3 (awarded to N.S.), CSC Scholarship and Spackman Award (L.B.), Total Energies E&P (H.S.), NSF-EAR grant 2051199 (A.C.), and Grant No. SKLOG202115. This work was performed at GeoSoilEnviroCARS (The University of Chicago, Sector 13), Advanced Photon Source (APS), Argonne National Laboratory. GeoSoilEnviroCARS is supported by the National Science Foundation – Earth Sciences (EAR – 1634415). This research used resources of the Advanced Photon Source, a U.S. Department of Energy (DOE) Office of Science User Facility operated for the DOE Office of Science by Argonne National Laboratory under Contract No. DE-AC02-06CH11357.

Appendix A. Supplementary material

Supplementary material to this article can be found online at https://doi.org/10.1016/j.gca.2022.09.035.

References

- Algeo, T.J., Lyons, T.W., 2006. Mo-total organic carbon covariation in modern anoxic marine environments: Implications for analysis of paleoredox and paleohydrographic conditions. Paleoceanography 21.
- Algeo, T.J., Maynard, J.B., 2004. Trace-element behavior and redox facies in core shales of Upper Pennsylvanian Kansas-type cyclothems. Chem. Geol. 206, 289–

- Algeo, T.J., Tribovillard, N., 2009. Environmental analysis of paleoceanographic systems based on molybdenum-uranium covariation. Chem. Geol. 268, 211– 225
- Ardakani, O.H., Hlohowskyj, S.R., Chappaz, A., Sanei, H., Liseroudi, M.H., Wood, J.M., 2020. Molybdenum speciation tracking hydrocarbon migration in fine-grained sedimentary rocks. Geochim. Cosmochim. Acta 283, 136–148.
- Aycard, M., Derenne, S., Largeau, C., Mongenot, T., Tribovillard, N., Baudin, F., 2003. Formation pathways of proto-kerogens in Holocene sediments of the upwelling influenced Cariaco Trench, Venezuela. *Org. Geochem.* 34, 701–718.
- Bennett, W.W., Lombi, E., Burton, E.D., Johnston, S.G., Kappen, P., Howard, D.L., Canfield, D.E., 2018. Synchrotron X-ray spectroscopy for investigating vanadium speciation in marine sediment: limitations and opportunities. J. Anal. At. Spectrom. 33, 1689–1699.
- Bharati, S., Patience, R.L., Larter, S.R., Standen, G., Poplett, I.J., 1995. Elucidation of the Alum Shale kerogen structure using a multi-disciplinary approach. Org. Geochem. 23, 1043–1058.
- Bian, L., Schovsbo, N.H., Chappaz, A., Zheng, X., Nielsen, A.T., Ulrich, T., Wang, X., Dai, S., Galloway, J.M., Małachowska, A., Xu, X., Sanei, H., 2021. Molybdenum-uranium-vanadium geochemistry in the lower Paleozoic Alum Shale of Scandinavia: Implications for vanadium exploration. Int. J. Coal Geol. 239, 103730.
- Bian, L., Chappaz, A., Schovsbo, N.H., Nielsen, A.T., Sanei, H., 2022. High mercury enrichments in sediments from the Baltic continent across the late Cambrian: Controls and implications. Chem. Geol. 599, 120846.
- Breit, G.N., Wanty, Ř.B., 1991. Vanadium accumulation in carbonaceous rocks: a review of geochemical controls during deposition and diagenesis. Chem. Geol. 91, 83–97.
- Chen, X., Li, S., Newby, S.M., Lyons, T.W., Wu, F., Owens, J.D., 2022. Iron and manganese shuttle has no effect on sedimentary thallium and vanadium isotope signatures in Black Sea sediments. Geochim. Cosmochim. Acta 317, 218–233.
- Chételat, J., Nielsen, S.G., Auro, M., Carpenter, D., Mundy, L., Thomas, P.J., 2021.
 Vanadium stable isotopes in biota of terrestrial and aquatic food chains.
 Environ. Sci. Technol. 55, 4813–4821.
- Emerson, S.R., Huested, S.S., 1991. Ocean anoxia and the concentrations of molybdenum and vanadium in seawater. Mar. Chem. 34, 177–196.
- Fan, H., Ostrander, C.M., Auro, M., Wen, H., Nielsen, S.G., 2021. Vanadium isotope evidence for expansive ocean euxinia during the appearance of early Ediacaran biota. Earth Planet. Sci. Lett. 567, 117007.
- Gill, B.C., Lyons, T.W., Young, S.A., Kump, L.R., Knoll, A.H., Saltzman, M.R., 2011. Geochemical evidence for widespread euxinia in the Later Cambrian ocean. Nature 469, 80–83.
- Gill, B.C., Dahl, T.W., Hammarlund, E.U., LeRoy, M.A., Gordon, G.W., Canfield, D.E., Anbar, A.D., Lyons, T.W., 2021. Redox dynamics of later Cambrian oceans. Palaeogeogra. Palaeoclimatol. Palaeoecol. 581, 110623.
- Gustafsson, J.P., 2019. Vanadium geochemistry in the biogeosphere–speciation, solid-solution interactions, and ecotoxicity. Appl. Geochem. 102, 1–25.
- Hlohowskyj, S.R., Chappaz, A., Dickson, A.J., 2021. Molybdenum as a paleoredox Proxy: Past, Present and Future. Elements in Geochemical Tracers in Earth System Science. Cambridge University Press.
- Hobson, A.J., Stewart, D.I., Bray, A.W., Mortimer, R.J., Mayes, W.M., Riley, A.L., Rogerson, M., Burke, I.T., 2018. Behaviour and fate of vanadium during the aerobic neutralisation of hyperalkaline slag leachate. Sci. Total Environ. 643, 1191–1199.
- Huang, J.H., Huang, F., Evans, L., Glasauer, S., 2015. Vanadium: Global (bio)geochemistry. Chem. Geol. 417, 68–89.
- Kelley, K.D., Scott, C., Polyak, D.E., Kimball, B.E., 2017. Vanadium (No. 1802-U). US Geological Survey. In: Schulz, K.J., DeYoung, J.H., Seal, R.R., Bradley, D.C. (Eds.), Critical Mineral Resources of the United States: Economic and Environmental Geology and Prospects for Future Supply. Geological Survey.
- Kok, M.D., Schouten, S., Damsté, J.S.S., 2000. Formation of insoluble, nonhydrolyzable, sulfur-rich macromolecules via incorporation of inorganic sulfur species into algal carbohydrates. Geochim. Cosmochim. Acta 64, 2689–2699.
- Kunert, A., Clarke, J., Kendall, B., 2020. Molybdenum Isotope Constraints on the Origin of Vanadium Hyper-Enrichments in Ediacaran-Phanerozoic Marine Mudrocks. Minerals 10, 1075.
- Lehmann, B., Nägler, T.F., Holland, H.D., Wille, M., Mao, J., Pan, J., Ma, D., Dulski, P., 2007. Highly metalliferous carbonaceous shale and Early Cambrian seawater. Geology 35, 403–406.
- Loog, A., Petersell, V., 1995. Authigenic siliceous minerals in the Tremadoc grantolitic argillite of Estonia, Proc. Est. Acad. Sci. Geol. 44, 26–32.
- graptolitic argillite of Estonia. Proc. Est. Acad. Sci. Geol. 44, 26–32. Loog, A., Kurvits, T., Aruvali, J., Petersell, V., 2001. Grain size analysis and mineralogy of the Tremadocian Dictyonema shale in Estonia. Oil Shale 18, 281–297.
- Machel, H.G., 2001. Bacterial and thermochemical sulfate reduction in diagenetic settings—old and new insights. Sediment. Geol. 140, 143–175.
- McCann, N., Wagner, M., Hasse, H., 2013. A thermodynamic model for vanadate in aqueous solution–equilibria and reaction enthalpies. Dalton Trans. 42, 2622–2628.
- Moore, E.K., Hao, J., Spielman, S.J., Yee, N., 2020. The evolving redox chemistry and bioavailability of vanadium in deep time. Geobiology 18, 127–138.
- Morford, J.L., Emerson, S., 1999. The geochemistry of redox sensitive trace metals in sediments. Geochim. Cosmochim. Acta 63, 1735–1750.
- Nedrich, S.M., Chappaz, A., Hudson, M.L., Brown, S.S., Burton Jr, G.A., 2018. Biogeochemical controls on the speciation and aquatic toxicity of vanadium and other metals in sediments from a river reservoir. Sci. Total Environ. 612, 313–320.

- Nielsen, S.G., Prytulak, J., Halliday, A.N., 2011. Determination of precise and accurate 51V/50V isotope ratios by MC-ICP-MS, Part 1: Chemical separation of vanadium and mass spectrometric protocols. Geostand. Geoanal. Res. 35, 293–306.
- Nielsen, A.T., Schovsbo, N.H., 2007. Cambrian to basal Ordovician lithostratigraphy in southern Scandinavia. Bull. Geol. Soc. Denmark 53, 47–92.

 Nielsen, A.T., Schovsbo, N.H., 2011. The Lower Cambrian of Scandinavia:
- Nielsen, A.T., Schovsbo, N.H., 2011. The Lower Cambrian of Scandinavia: depositional environment, sequence stratigraphy and palaeogeography. Earth Sci. Rev. 107, 207–310.
- Nielsen, A.T., Schovsbo, N.H., 2015. The regressive Early-Mid Cambrian 'Hawke Bay Event'in Baltoscandia: epeirogenic uplift in concert with eustasy. Earth Sci. Rev. 151, 288–350.
- Nielsen, S.G., 2020. Vanadium isotopes: A proxy for ocean oxygen variations. In: Lyons, T., Turchyn, A., Reinhard, C. (Eds.), Elements in Geochemical Tracers in Earth System Science. Cambridge University Press.
- O'Loughlin, E.J., Boyanov, M.I., Kemner, K.M., 2021. Reduction of vanadium (V) by iron (II)-bearing minerals. Minerals 11, 316.
- Peacor, D.R., Coveney Jr, R.M., Zhao, G., 2000. Authigenic illite and organic matter: The principal hosts of vanadium in the Mecca Quarry Shale at Velpen, Indiana. *Clays Clay Miner.* 48, 311–316.
- Petersen, H.I., Schovsbo, N.H., Nielsen, A.T., 2013. Reflectance measurements of zooclasts and solid bitumen in lower Paleozoic shales, southern Scandinavia: Correlation to vitrinite reflectance. Int. J. Coal Geol. 114, 1–18.
- Rickard, D., Luther, G.W., 2007. Chemistry of iron sulfides. Chem. Rev. 107, 514–562. Sahoo, S.K., Planavsky, N.J., Kendall, B., Wang, X., Shi, X., Scott, C., Anbar, A.D., Lyons, T.W., Jiang, G., 2012. Ocean oxygenation in the wake of the Marinoan glaciation. Nature 489, 546–549.
- Sahoo, S.K., Planavsky, N.J., Jiang, G., Kendall, B., Owens, J.D., Wang, X., Shi, X., Anbar, A.D., Lyons, T.W., 2016. Oceanic oxygenation events in the anoxic Ediacaran ocean. Geobiology 14, 457–468.
- Sanei, H., 2020. Genesis of solid bitumen. Sci. Rep. 10, 1-10.
- Sanei, H., Petersen, H.I., Schovsbo, N.H., Jiang, C., Goodsite, M.E., 2014. Petrographic and geochemical composition of kerogen in the Furongian (U. Cambrian) Alum Shale, central Sweden: Reflections on the petroleum generation potential. Int. J. Coal Geol. 132, 158–169.
- Schlesinger, W.H., Klein, E.M., Vengosh, A., 2017. Global biogeochemical cycle of vanadium. Proc. Natl. Acad. Sci. U.S.A. 114, E11092–E11100.
- Schovsbo, N.H., 2001. Why barren intervals? A taphonomic case study of the Scandinavian Alum Shale and its faunas. Lethaia 34, 271–285.
- Schovsbo, N.H., Nielsen, A.T., Gautier, D.L., 2014. The lower Paleozoic shale gas play in Denmark. GEUS Bull. 31, 19–22.
- Schulz, H.M., Yang, S., Schovsbo, N.H., Rybacki, E., Ghanizadeh, A., Bernard, S., Mahlstedt, N., Krüger, M., Amann-Hildebrandt, A., Krooss, B.M., Meier, T., 2021. The Furongian to Lower Ordovician Alum Shale Formation in conventional and unconventional petroleum systems in the Baltic Basin–A review. Earth Sci. Rev. 218, 103674.
- Schuth, S., Brüske, A., Hohl, S.V., Jiang, S.Y., Meinhardt, A.K., Gregory, D.D., Viehmann, S., Weyer, S., 2019. Vanadium and its isotope composition of river water and seawater: Analytical improvement and implications for vanadium isotope fractionation. Chem. Geol. 528, 119261.
- Scotese C. R., 2001. Atlas of Earth History (PALEOMAP Project, 2001).
- Scott, C., Lyons, T.W., 2012. Contrasting molybdenum cycling and isotopic properties in euxinic versus non-euxinic sediments and sedimentary rocks: Refining the paleoproxies. Chem. Geol. 324, 19–27.
- Scott, C., Slack, J.F., Kelley, K.D., 2017. The hyper-enrichment of V and Zn in black shales of the Late Devonian-Early Mississippian Bakken Formation (USA). Chem. Geol. 452, 24–33.
- Sørensen, A.L., Nielsen, A.T., Thibault, N., Zhao, Z., Schovsbo, N.H., Dahl, T.W., 2020. Astronomically forced climate change in the late Cambrian. Earth Planet. Sci. Lett. 548, 116475.

- Sturesson, U.L.F., Popov, L.E., Holmer, L.E., Bassett, M.G., Felitsyn, S., Belyatsky, B., 2005. Neodymium isotopic composition of Cambrian-Ordovician biogenic apatite in the Baltoscandian Basin: implications for palaeogeographical evolution and patterns of biodiversity. Geo. Mag. 142, 419–439.
- Sweere, T., van den Boorn, S., Dickson, A.J., Reichart, G.J., 2016. Definition of new trace-metal proxies for the controls on organic matter enrichment in marine sediments based on Mn Co, Mo and Cd concentrations. Chem. Geol. 441, 235– 245
- Taylor, S.R., McLennan, S.M., 1985. The continental crust: its composition and evolution. Oxford, Blackwell, UK, p. 312.
- Tegelaar, E.W., De Leeuw, J.W., Derenne, S., Largeau, C., 1989. A reappraisal of kerogen formation. Geochim. Cosmochim. Acta 53, 3103–3106.
- Tessin, A., Chappaz, A., Hendy, I., Sheldon, N.D., 2019. Molybdenum speciation as a paleo-redox proxy: A case study from Late Cretaceous Western Interior Seaway black shales. Geology 49, 59–62.
- Tribovillard, N., Algeo, T.J., Lyons, T., Riboulleau, A., 2006. Trace metals as paleoredox and paleoproductivity proxies: an update. Chem. Geol. 232, 12–32. Vessey, C.J., Lindsay, M.B., 2020. Aqueous vanadate removal by iron (II)-bearing
- phases under anoxic conditions. Environ. Sci. Technol. 54, 4006–4015. Vessey, C.J., Schmidt, M.P., Abdolahnezhad, M., Peak, D., Lindsay, M.B., 2020.
- Vessey, C.J., Schmidt, M.P., Abdolahnezhad, M., Peak, D., Lindsay, M.B., 2020. Adsorption of (poly) vanadate onto ferrihydrite and hematite: An in situ ATR– FTIR study. ACS Earth Space Chem. 4, 641–649.
- Wagner, M., Chappaz, A., Lyons, T.W., 2017. Molybdenum speciation and burial pathway in weakly sulfidic environments: Insights from XAFS. Geochim. Cosmochim. Acta 206, 18–29.
- Wakeham, S.G., 1995. Lipid biomarkers for heterotrophic alteration of suspended particulate organic matter in oxygenated and anoxic water columns of the ocean. Deep Sea Res. Part I: Oceanogr. Res. Pap. 42, 1749–1771.
- Wanty, R.B., Goldhaber, M.B., 1992. Thermodynamics and kinetics of reactions involving vanadium in natural systems: Accumulation of vanadium in sedimentary rocks. Geochim. Cosmochim. Acta 56, 1471–1483.
- Waples, D.W., 2013. Geochemistry in Petroleum Exploration. Springer Science & Business Media.
- Więcław, D., Kotarba, M.J., Kosakowski, P., Kowalski, A., Grotek, I., 2010. Habitat and hydrocarbon potential of the lower Paleozoic source rocks in the Polish part of the Baltic region. Geol. Q. 54, 159–182.
- Wilson, S.A., Weber, J.H., 1979. An EPR study of the reduction of vanadium (V) to vanadium (IV) by fulvic acid. Chem. Geol. 26, 345–354.
- Wu, F., Qin, T., Li, X., Liu, Y., Huang, J.H., Wu, Z., Huang, F., 2015. First-principles investigation of vanadium isotope fractionation in solution and during adsorption. Earth Planet. Sci. Lett. 426, 216–224.
- Wu, F., Owens, J.D., Huang, T., Sarafian, A., Huang, K.F., Sen, I.S., Horner, T.J., Blusztajn, J., Morton, P., Nielsen, S.G., 2019. Vanadium isotope composition of seawater. Geochim. Cosmochim. Acta 244, 403–415.
- Wu, F., Owens, J.D., Scholz, F., Huang, L., Li, S., Riedinger, N., Peterson, L.C., German, C.R., Nielsen, S.G., 2020. Sedimentary vanadium isotope signatures in low oxygen marine conditions. Geochim. Cosmochim. Acta 284, 134–155.
- Yang, Z., Gould, E.S., 2003. Reactions of vanadium (IV) and (V) with s2 metal-ion reducing centers. Dalt. Trans. 20, 3963–3967.
- Zhao, Z., Ahlberg, P., Thibault, N., Dahl, T.W., Schovsbo, N.H., Nielsen, A.T., 2022. High-resolution carbon isotope chemostratigraphy of the middle Cambrian to lowermost Ordovician in southern Scandinavia: Implications for global correlation. Glob. Planet. Change., 103751
- Zheng, X., Schovsbo, N.H., Bian, L., Luo, Q., Zhong, N., Rudra, A., Goodarzi, F., Sanei, H., 2021. Alteration of organic macerals by uranium irradiation in lower Paleozoic marine shales. Int. J. Coal Geol. 239, 103713.